A PIV AND CFD INVESTIGATION OF CAVITY FLOWS IN THE TRANSONIC FLOW REGIME

S A Ritchie, N J Lawson* and K Knowles
Aeromechanical Systems Group
Department of Aerospace, Power and Sensors
Cranfield University, RMCS Shrivenham
Swindon, Wiltshire, SN6 8LA
Email: s.a.ritchie@rmcs.cranfield.ac.uk

Keywords: *cavity flow, transonic, PIV, CFD*

Abstract

Particle image velocimetry (PIV) measurements are presented from rectangular cavities of different length-to-depth ratios at a Mach number of 0.85 in the RMCS transonic wind tunnel. The measurements are made in l/h=5 and l/h=14 cavities in order to encompass the open and closed flow regimes. The time-averaged two-dimensional PIV results are compared with time-averaged two-dimensional URANS CFD predictions. Streamwise and vertical velocity components are compared for three depths within the cavity; y/h=0.25, y/h=0.5 and y/h=0.75. Good agreement is found in the mean flow structure between the experimental and numerical data collected for the study. The maximum flow velocities extracted from the PIV data for the 'open' cavity case are generally lower than those predicted by the CFD model. The maximum flow velocities extracted from the 'closed' cavity PIV data are generally higher than the values predicted by the CFD model.

Nomenclature

h	cavity depth
l	cavity length
M	Mach number
N	Number of samples
V	local velocity magnitude
u	streamwise velocity component
v	vertical velocity component
w	cavity width
x	streamwise direction
y	depthwise direction
z	spanwise direction

Subscripts

∞	Freestream condition

Cavity geometries are consistent with the standard ESDU cavity notation [1] as seen in **Figure 1**.

1 Introduction

The advent of stealth aircraft, and the corresponding requirement for aircraft designs to have reduced radar signatures, has prompted the need for weapons to be stored and released internally from bomb bays. Once the bomb bay doors are opened a cavity flow is produced. Cavity flows can be defined as one of two main types, primarily dependent on the length-to-depth ratio (L/D) of the cavity [2][3]. "Open" cavity flows occur in cavities with L/D<10 (**Fig 2**) and are characterised by strong pressure oscillations which lead to noise radiation (often in excess of 170dB), structural vibration and high levels of heat transfer at the trailing edge. "Closed" cavity flows occur in cavities with

* Present address: School of Engineering, Cranfield University, Cranfield, Bedfordshire, MK43 0AL, UK.

L/D>13 and are regarded as quasi-steady flows (**Fig 3**). The pressure distribution along the roof of a "closed" cavity shows a large longitudinal pressure gradient that causes a large increase in pressure drag and can lead to store separation difficulties. Cavity geometries in the range 10<L/D<13 are described as "transitional" and here the cavity flows exhibit a combination of "open" and "closed" flow features.

Many previous studies of cavity flows have concentrated on the time-averaged and unsteady measurement of the flow using static pressure taps on the surfaces and qualitative visualisation techniques like schlieren imagery and oil flow visualisation [4][5][6]. The results of these studies have typically been compared to numerical models with mixed success [7][8]. There is currently limited data available on the actual flowfield within different cavity geometries under transonic conditions. Advanced optical techniques such as particle image velocimetry (PIV) [9] now offer the potential to record quantitative velocity data from transonic and supersonic flows [10].

2 Experimentation

2.1 Transonic Wind Tunnel

All tests were conducted using the Royal Military College of Science (RMCS) transonic wind tunnel (TWT), a schematic of which is seen in **Figure 4**. The tunnel has a working section of 206mm (height) by 229mm (width). The facility is a closed circuit ejector driven tunnel supplied with air from two Howden screw-type compressors. The compressors supply air at up to 7 bar(g), which is dried and stored in a 34m³ reservoir. The stored air is sufficient to run the tunnel at Mach 0.85 (the test condition for the present PIV measurements) for 15 seconds.

Cavity models can be mounted on one or other of the working section side walls. For the PIV measurements an all-glass cavity was mounted from the underside of a raised flat plate which also acted as a splitter for the tunnel wall boundary layer. Data could not be acquired for the first 2mm of the cavity depth due to the presence of the splitter plate. Similarly, the wind tunnel design does not allow the freestream flow to be measured using PIV, because of a lack of optical access.

A custom-built seeding system injected water particles of 5-10μm diameter into the contraction section to seed the flow (**Figure 5a**). The seeder supplied a rake of three impactor atomiser nozzles with water pressurised to 2000psi.

2.2 PIV System

The PIV system consisted of a Dantec FlowMap 500 hardware box, a Kodak ES1.0 megapixel CCD camera and a New Wave Gemini Nd:YAG double pulsed laser. The Kodak ES1.0 camera frame rate and laser repetition rate allowed data to be recorded at up to 15Hz. The light sheet was projected into the cavity through the glass floor and was oriented along the cavity centreline. The seeded light sheet was viewed via a surface coated mirror angled at 45° to the cavity right side wall which provided a field of view normal to the light sheet. The exact details of the set up can be seen in **Figure 5b**. PIV data processing was initially undertaken using TSI's Insight software, which uses the Hart algorithm [11]. The data were also processed using an in-house code based on the correlation algorithm proposed by Meinhart et al [12]. The in-house code produces time-averaged flow fields only, but has the advantage of averaging the correlation peaks in each interrogation region instead of averaging the resulting vectors. This different approach to time averaging the data results in a higher signal to noise ratio from data where seeding levels are low. However, the resolution of this technique is reduced compared with the Hart algorithm which, given a suitable image with high seeding levels, can extract multiple vectors from each interrogation region. Table 1 lists the details of the processing variables for the different cavity geometries tested.

Cavity Geometry	*l/h=5*	*l/h=14*
TSI Primary Correlation Window Size (pixels)	32x32	16x16
TSI Secondary Correlation Window Size (pixels)	16x16	8x8
TSI Maximum Search Length (pixels)	8	8
TSI Vectors per Image	9600	3904
In-house Primary Correlation Window Size (pixels)	32x32	16x16
In-house window overlap (pixels)	24	4
In-house Maximum Search Length (pixels)	8	4
In-house Vectors per Image	1464	450

Table 1 PIV Processing Details

3 Numerical Modelling

Computational modelling was performed using the commercially-available CFD code Fluent. Computational grids of the cavity geometries were constructed using the grid-generation package GAMBIT. The domains for the cavities were sized at 500mm long to correspond to the size of the test rig flat plate and 230mm high to correspond to the TWT test section width.

The predictions were made using the segregated implicit solver with the realizable k-ε turbulence model. This particular turbulence model was chosen as it has been previously used in a number of studies involving flows with high shear and regions of recirculation and has been shown to be more effective for flows with regions of flow impingement and recirculation than the standard k-ε model [13]. The segregated implicit solver was chosen over the coupled implicit solver as it is less memory intensive and hence solutions can be attained more quickly. The segregated solver also offers better convergence performance than the coupled solver for the cases considered. The CFD predictions were computed on Linux workstations and with the available resources a single time step was computed in approximately 20-25 seconds.

4 Results

4.1 PIV Data

The PIV system acquires a maximum of 70 image pairs per tunnel run at a 15Hz sampling rate which is equivalent to the maximum laser cavity repetition rate. These datasets were processed into instantaneous vector maps and then into mean vector maps using the TSI code and directly into mean vector maps using the in-house code. The flow data were compared with the time-averaged URANS CFD predictions. Given a sample size of N = 70 and the random nature of the PIV sample, statistically the results will have a 12% uncertainty in the mean vector values as the component of uncertainty falls as $1/\sqrt{N}$ [14]. In order to reduce the uncertainty in the measurements, the image pairs from a number of tunnel runs were added together to generate the time-averaged vector maps from a much larger number of samples. Based on a sample size of N=700 image pairs, the uncertainty in the measurement has been estimated to be 3.7%.

Open Cavity (l/h=5)

As previously stated, time-averaged flow fields were extracted from the PIV data using the commercial TSI correlation code and an in-house correlation code. The resultant vector maps for the commercial and in-house codes can be seen in **Figures 6 and 7** respectively. The number of vectors in the figures has been reduced by 50% to increase the clarity of the flow structures. In both cases the structure of the flow field closely matches the expected large single recirculation region which is characteristic of the mean flow field in an open cavity. The low concentration of seeding in the upstream region of the cavity affects the quality of data extracted by the TSI code but has a

lesser effect on the data processed with the in-house code due to the nature of the algorithm. The position of the centre of recirculation within the cavity is extracted at slightly different locations. The TSI code shows the centre of recirculation to be positioned at x/l=0.4 whilst the in-house code shows the centre to be positioned x/l=0.5. The shear layer which bridges the cavity is visibly deflected into the cavity near the downstream wall and as a result the flow in this region is faster than elsewhere in the cavity.

Closed Cavity (l/h=14)

The time-averaged flow fields extracted from the l/h=14 PIV data can be seen in **Figures 8 and 9** for the TSI and in-house codes respectively. Examination of the flow field structure for the two data sets shows that the flow exhibits good similarity to the expected mean flow field described in the literature. The flow enters the cavity and traps a region of expanded flow in the upstream half of the cavity before flowing along the cavity floor between x/l=0.5-0.7 and then turning out of the cavity near the downstream end and trapping a small region of compressed flow.

4.2 Time-averaged CFD Data

The time-averaged CFD flow fields are constructed from 20000 time steps of 5μs to give 0.1 seconds of flow time for both the l/h=5 and l/h=14 cases.

Open Cavity (l/h=5)

The flow field displays a large single recirculation region within the cavity which is expected from the literature and is consistent with the PIV flow fields. However, the CFD flow field has a region of flow on the floor near the downstream wall in which the flow velocity is much greater than that extracted from the PIV data. This increased flow velocity is due to the addition of mass to the cavity at the downstream wall where the shear layer is below the level of the trailing edge. The flow in the first 15% of the cavity length has a low-speed ($0\pm20ms^{-1}$) compared to elsewhere in the cavity. This is consistent with the PIV data showing that the recirculation does not fill the entire cavity. Literature suggests that the flow in this region contains a contra-rotating vortex although this is not confirmed or otherwise by the PIV and CFD data.

Closed Cavity (l/h=14)

The flow structure is consistent with that expected from the literature. A region of flow is present on the cavity floor from 10-60% of the cavity length which is of increased velocity compared with the surrounding flow. This is not present in the PIV data; however, this may be due to the high spatial gradient in this region adversely affecting the data extracted from the PIV images.

5 Discussion

In order to quantitatively compare the PIV and CFD data from the three flow fields, profiles of the streamwise and vertical velocity components were extracted along the cavity at y/d=0.25 (75% of cavity height from floor), y/d=0.5 (50% of cavity height from floor) and y/d=0.75 (25% of cavity height from floor).

5.1 Open Cavity (l/h=5)

Figures 10 and 11 show the u velocity component from the cavity at y/d=0.25 and y/d=0.75 respectively. At y/d=0.25 the peak velocity extracted by the TSI code closely matches the CFD predicted velocity in terms of both value and position. The in-house code shows peak values of approximately $60ms^{-1}$ which is 7% less of freestream values ($\approx20ms^{=1}$) than the TSI and CFD values. It can be seen from the three vector fields that the CFD predicts the recirculation centre at x/l=0.7 whilst

the two PIV codes show the centre of recirculation to be located between x/l=0.4-0.5.

The CFD predicts peak velocities up to -125m^{-1} in u at y/d=0.75. The region of increased flow velocity on the floor near the downstream wall in the CFD prediction is not mirrored in the PIV data which suggests that the large increase In flow velocity as the flow travels down the downstream wall and the large decrease in flow velocity as the flow travels upstream along the cavity floor cannot be extracted from the PIV data. Keane and Adrian [15] recommend that a seeding particle should travel no further than 25-30% of the interrogation window size between laser pulses in order to extract high quality data. However, in flows with a high degree of shear and swirl, large velocity gradients may exist which apply large accelerations on the seeding particles. This results in a degradation of the correlation signal from the PIV images with a subsequent loss in data yield. Smaller interrogation regions will reduce this effect but pulse separations must be correspondingly reduced which will degrade accuracy and dynamic range. Thus a balance must be sort between accuracy, dynamic range and data yield. Given the minimum resolution of the data processing system is around 0,1 pixel the expected dynamic range is around 50, Thus some flow features will be incorrectly extracted; this seems to be the case in the region along the cavity floor.

5.2 Closed Cavity (l/h=14)

Figures 12 and 13 show the u velocity component profiles at y/d=0.25 and y/d=0.5. The streamwise velocity profiles extracted from the three datasets all show close agreement in terms of the trends described by the data. At y/d=0.25, the CFD and the PIV data processed with the in-house code show excellent agreement in trend and velocity values whilst the TSI processed data follows the trend but the velocity values are up to 24% of freestream values (≈70ms^{-1}) lower than the CFD and in-house PIV values.

At y/d=0.5, the PIV data and the CFD data follow similar trends. The CFD peak velocities, however, are approximately 10% of freestream values lower (≈25-30ms^{-1}) than the values extracted from the PIV data.

5.3 General

Comparison of the flow structures and velocity trends for the two different cavity geometries shows that whilst the PIV technique is capable of extracting the mean flow structure accurately, the velocities which can be extracted are affected by the limitations of the processing code in terms of maximum particle displacement and high levels of swirl and shear.

Improvements to the PIV data can be made using the two current processing codes by dividing the flow field into a number of smaller flow regions based upon the expected flow velocities. These regions can then be processed with smaller maximum displacements and smaller interrogation regions. This technique may help to improve the flow velocity values within the cavity. However, complex flow structures may still remain difficult to extract successfully. An alternative correlation code is available which deforms the interrogation window in the second frame of an image pair in order to try and follow strong spatial gradients within the flow. This will be the subject of a future study.

PIV measurements in high-speed flows with high frequency phenomena such as open cavity flows, which lead to rapid changes in speed and direction, may suffer from delay in the response of the seeding to these changes. This can cause measured peak velocities to be artificially reduced. Dring [16] provides a method to estimate the error in velocity caused by the seeding lag for either a step deceleration or an exponential acceleration. For example, with seeding particles between 5-10μm in diameter, a

particle density of 1000kgm^{-3} and an exponential acceleration from 20-150ms^{-1} in 20mm (which is representative of the flow velocity increase near the downstream wall of the open cavity), the particle Stokes number will vary from 0.009 to 0.036 which corresponds to a predicted error of 6 to 10%. This can only be reduced by using smaller and particles as fluid particles are preferred. Smaller particles require greater laser power or camera sensitivity. But recent advances in camera technology should allow this.

The acquisition of PIV data from cavity flows at transonic speeds has proved to be most challenging in terms of both rig design and data acquisition. The RMCS TWT layout is such that major alterations to improve optical access are not possible. Any improvement in access for lasers had to be achieved through the design of the cavity rig.

Access for light sheet and imaging optics in the RMCS TWT is highly restricted due to the size of the tunnel test section. Hence PIV rig design is limited to attaching a fully or partially clear cavity to the outside of the tunnel wall as in the current design (**Fig 5**). The highly unsteady nature of the flow within the open cavity has proved to be difficult to capture with the image acquisition refresh rates available. The current acquisition rate of the CCD camera and Nd:YAG laser used for image acquisition is limited to 15Hz and as such is too low to fully resolve the flow structures associated with dominant frequencies of oscillation. Estimates from the modified Rossiter equation [17] place the frequencies of the first three modes of oscillation for the open cavity case at 460Hz, 1125Hz and 1795Hz. A time-resolved or cinematic PIV system with laser and camera repetition rates in the order of 2kHz would be required to properly resolve the first two frequencies of oscillation expected within the cavity.

5.4 Comparisons with Previous Work

Previous published studies relating to non-intrusive measurements of cavity flows are limited to work conducted by Esteve *et al* [18] and Unalmis *et al* [19]. In the first case, the PIV studies were conducted at low subsonic fllow-speeds and in the second case the measurements were restricted to flow visualisation using planar laser scattering (PLS). As such no direct comparisons can be made between previous work and the results presented here; it is believed no equivalent PIV studies for closed and transitional cavities at transonic speeds have been published in the open literature to date.

A considerable number of computational studies have been dedicated to modelling the flow over cavities at transonic speeds. A survey conducted by Grace [20] into computational techniques for cavity flow noise prediction covered many of the main studies to date. A more recent study of note includes predictions for an l/h=5 cavity for the same flow conditions as the current test conducted by Lawrie *et al* [21] using the SST k-ω turbulence model. The results from this study have been used as a basis for the development of the solutions contained within the current cavity flow study.

6 Conclusions

For the first time, time-averaged PIV and CFD results have been presented for open and closed cavity flows at transonic speeds. The comparison of time-averaged PIV data with URANS CFD predictions has proved the ability of PIV to be used as a tool for the analysis of the complex flow structures associated with cavity flows at transonic speeds. Whilst flow structures can be extracted using PIV, traditional correlation codes in which the interrogation window shape is fixed cannot extract data from regions containing high spatial gradients. This is most apparent in the l/h=5 cavity where the high-speed flow region on the floor, which is predicted by the CFD, is not extracted from the PIV images. This limitation

of the two codes used for this study can be overcome with the use of a new development in correlation codes whereby the interrogation region is deformed in order to track more effectively large particle displacements due to spatial gradients [22].

More detailed work is required to improve these results. The current study has shown that PIV can be used as a means for detailed analysis of cavity flows providing due attention is paid to optical access and seeding quality. Based on the PIV data processed for the current study, it is clear that whilst the results from time-averaged flow fields produce vector maps with flow structures similar to those defined in the cavity flow literature. Unfortunately the instantaneous vector maps are captured at too low a frame rate to be able to extract frequency information from the cavity. This can only be properly addressed by either 'phase-locking' the PIV acquisition to each of the oscillation frequencies or using a high-speed PIV system with a minimum of 2-3kHz capture rate to acquire time resolved flow data. Whilst 'phase-locked' acquisition can successfully extract flow data for a single frequency phenomenon, flows in which multiple frequencies of oscillation exist cannot be fully analysed. This suggests that future studies of 'open' cavity flows should be undertaken with high-speed PIV systems which can extract full time-wise behaviour from flows with multiple frequencies of oscillations.

Acknowledgements

The authors would like to thank the EPSRC and MBDA UK Ltd for their support of some of this work under the CASE award scheme. We would also like to thank Dr John Coath, Mr Roy Walker and Dr Mark Finnis of the Department of Aerospace, Power and Sensors and the workshops of the Engineering Systems Department at Shrivenham for their assistance with various aspects of this work.

References

[1] ESDU, (2002), "Drag of a rectangular planform cavity in a flat plate with a turbulent boundary layer for Mach numbers up to 3. Part II : Open and transitional flows", *ESDU 00007*,

[2] Charwat, A. F., Roos, J. N., Dewey, F. C., Jr., and Hitz, J.A (1961): *J. Aerosp. Sci.*, vol. 28,no.6, June, pp. 457—470.

[3] Stallings, R.J., et al., (1995) "Measurements of Store Forces and Moments and Cavity Pressures for a Generic Store in and Near a Box Cavity at Subsonic and Transonic Speeds" *NASA TM-4611*. NASA.

[4] Taborda, N.M., D. Bray, and K. Knowles, (2001) "Passive Control of Cavity Resonances in Tandem Configurations", *31st AIAA Fluid Dynamics Conference*, Anaheim, CA, 11-14 June 2001. Paper no. AIAA 2001-2770.

[5] Taborda, N., D. Bray, and K. Knowles, (2001) "Visualisation of Three-dimensional Cavity Flows", in *5th World Conference on Experimental Heat Transfer, Fluid Mechanics and Thermodynamics*. Thessaloniki, Greece.

[6] Garg, S. and L.N. Cattafesta III, (2001) "Quantitative Schlieren Measurements of Coherent Structures in a Cavity Shear Layer", *Experiments in Fluids*, (30): p. 123-134.

[7] Sinha, N., et al. (1998) "A Perspective on the Simulation of Cavity Aeroacoustics", in *36th Aerospace Sciences Meeting and Exhibit*. Reno, NV.

[8] Zhang, J., et al. (2001) "Experimental and Computational Investigation of Supersonic Cavity Flows", in *10th AIAA/NAL-NASDA-ISAS International Space Planes and Hypersonic Systems and Technologies Conference*. Tokyo.

[9] Adrian, R.J., (1991) "Particle Imaging Techniques for Experimental Fluid Mechanics", *Annual Review of Fluid Mechanics*, (23): p. 261-304.

[10] Lawson N.J., Page G., Halliwell N.A., Coupland J.M. (1999) "Application of Particle Image Velocity to a Small Scale de Laval Nozzle", *AIAA Journal* 37(7), p798-804.

[11] Hart, D., (2000), "PIV error correction." *Experiments in fluids*, 29, 13-22

[12] Meinhart, C., Wereley, S., and Santiago, J., (2000), "A PIV Algorithm for Estimating Time-Averaged Velocity Fields." *Journal of Fluids Engineering* **(122)**, 285-289.

[13] Prepared by WS Atkins Consultants and Members of the NSC (2002), "Best Practice Guidelines for Marine Applications of Computational Fluid Dynamics" http://pronet.wsatkins.co.uk/marnet/guidelines/guide.html/

[14] Coleman, H., and Steele, W., (1999), *Experimentation and uncertainty analysis for engineers*, John Wiley and Sons, Inc., New York.

[15] Keane, R., and Adrian, R., (1990), "Optimization of Particle Image Velocimeters. Part I: Double Pulsed Systems." *Measurement Science and Technology*, 1, 1202-1215.

[16] Dring, R., (1982), "Sizing criteria for laser anemometry particles." *Journal of Fluids Engineering*, 104, 15-17.

[17] Rossiter, J. E., (1964), "Wind tunnel experiments on the flow over rectangular cavities at subsonic and transonic speeds." Royal Aircraft Establishment.

[18] Esteve, M. J., Reulet, P., and Millan, P., (2000), "Flow field characterisation within a rectangular cavity", 10th International Symposium on the Applications of Laser Technology to Fluid Mechanics, Lisbon, Portugal.

[19] Unalmis, O. H., Clemens, N. T., and Dolling, D. S., (1999), "Planar Laser Imaging of a Supersonic Side Facing Cavity", *37th AIAA Aerospace Sciences Meeting and Exhibit*, Reno NV, January 11-14 1999.

[20] Grace, S., (2001), "An Overview of Computational Aeroacoustic Techniques Applied to Cavity Noise Prediction", *39th AIAA Aerospace Sciences Meeting and Exhibit*, Reno, NV.

[21] Lawrie, D., Nayyar, P., Badcock, K., Barakos, G., and Richards, B., (2003), "CFD Study of Cavity Flows", *CEAS Aerospace Aerodynamics Research Conference*, London, UK, 10-12 June 2003.

[22] Scarano, F., (2002), "Iterative Deformation Methods in PIV." *Measurement Science and Technology*, 13, R1-R19.

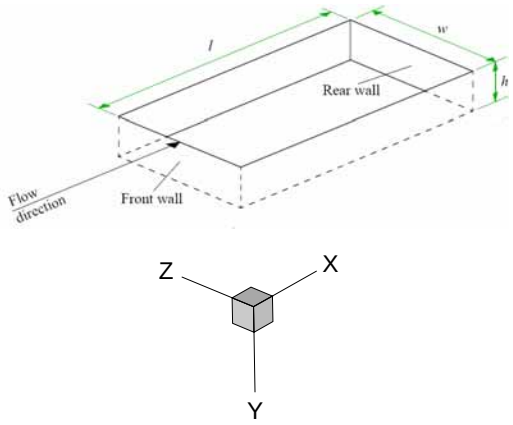

Fig 1 Standard ESDU cavity notations [1]

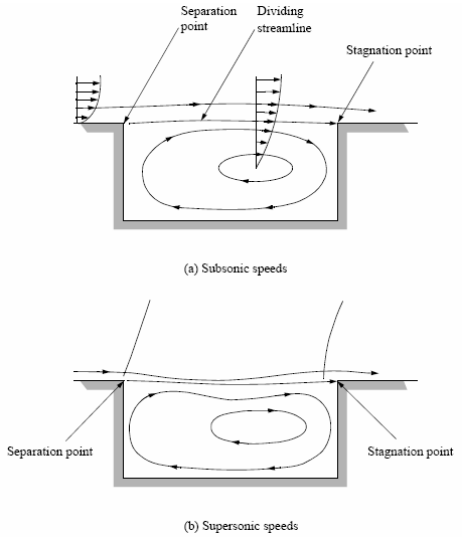

Fig 2 Mean flow features of open cavity flow [1]

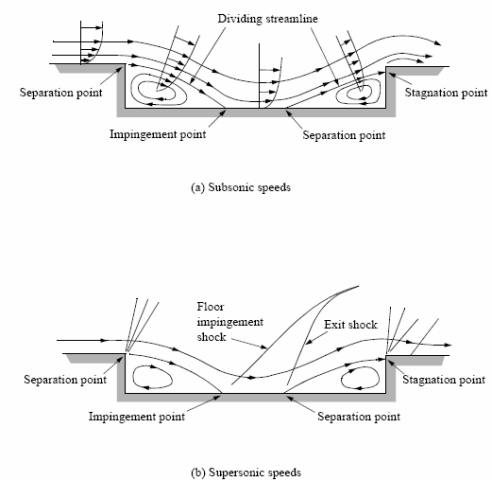

Fig 3 Mean flow features of closed cavity flow [1]

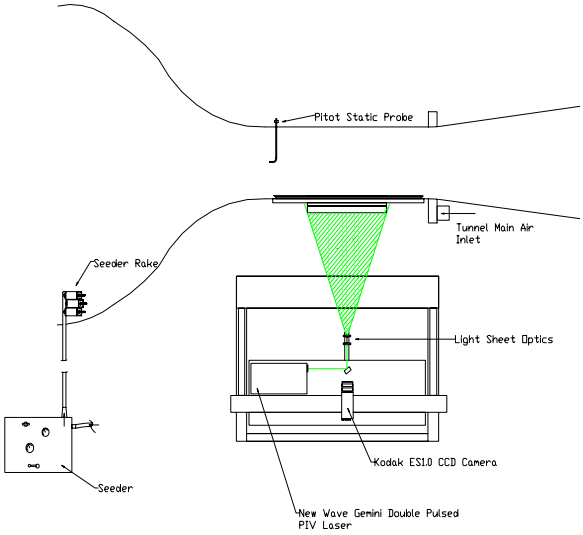

Figure 5a PIV Experimental Setup Top View

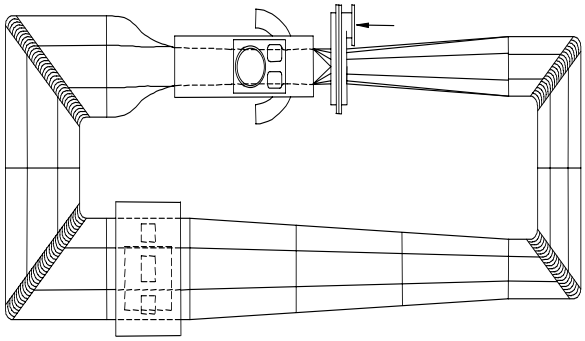

Fig 4 Layout of RMCS Shrivenham transonic wind tunnel

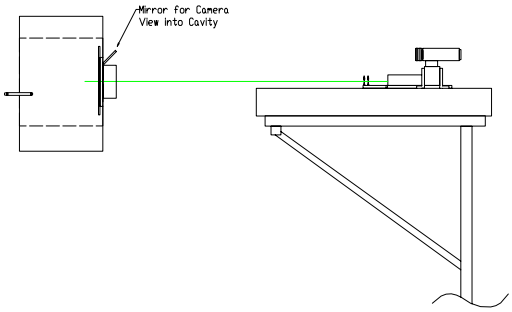

Figure 5b PIV Experimental Setup Side View

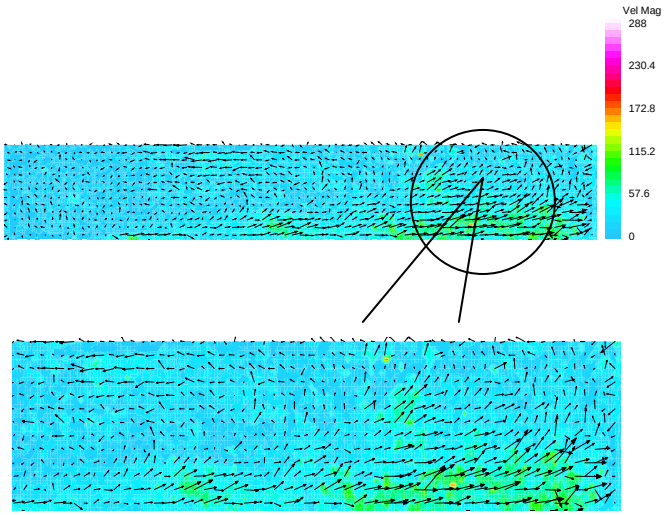

Figure 6 Mean PIV vector map using TSI correlation code – l/h=5

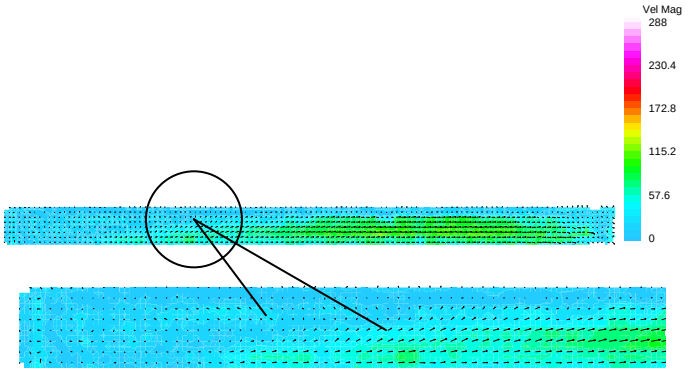

Figure 8 Mean PIV vector map using TSI correlation code – l/h=14

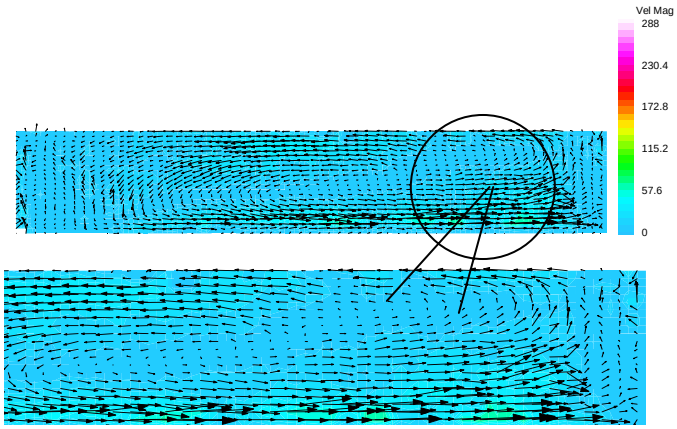

Figure 7 Mean PIV vector map using In-house correlation code – l/h=5

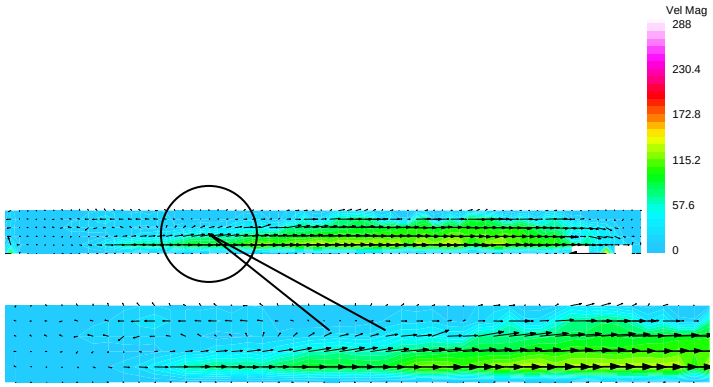

Figure 9 Mean PIV vector map using In-House correlation code - l/h=14

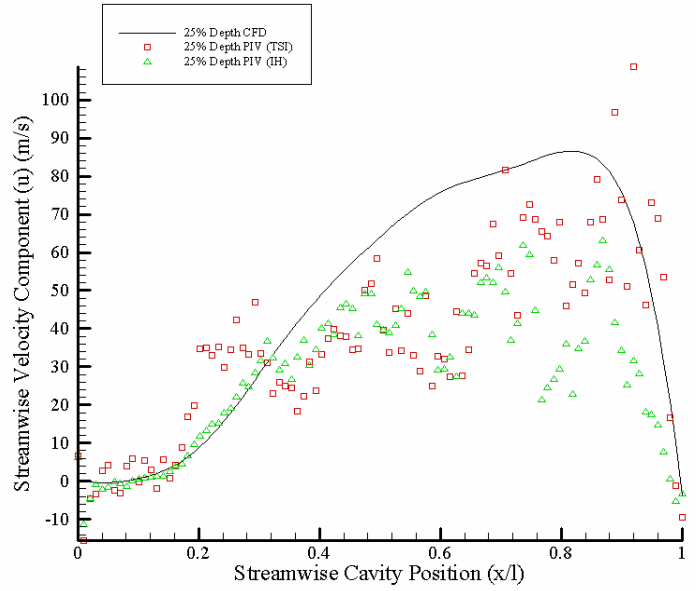

Figure 10 Streamwise Velocity Profile – l/h=5, y/d=0.25

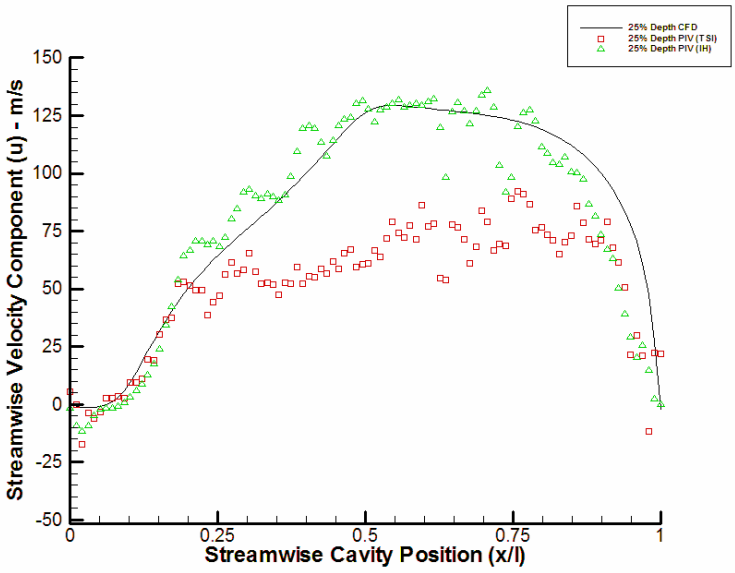

Figure 12 Streamwise Velocity Profile – l/h=14, y/d=0.25

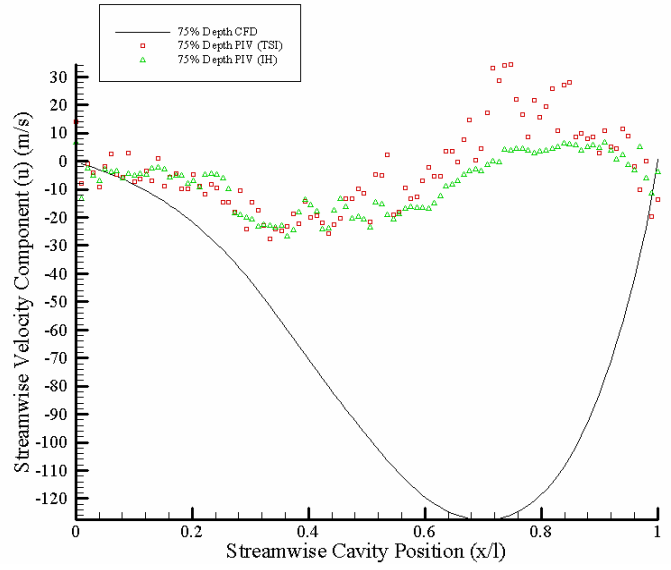

Figure 11 Streamwise Velocity Profile – l/h=5, y/d=0.75

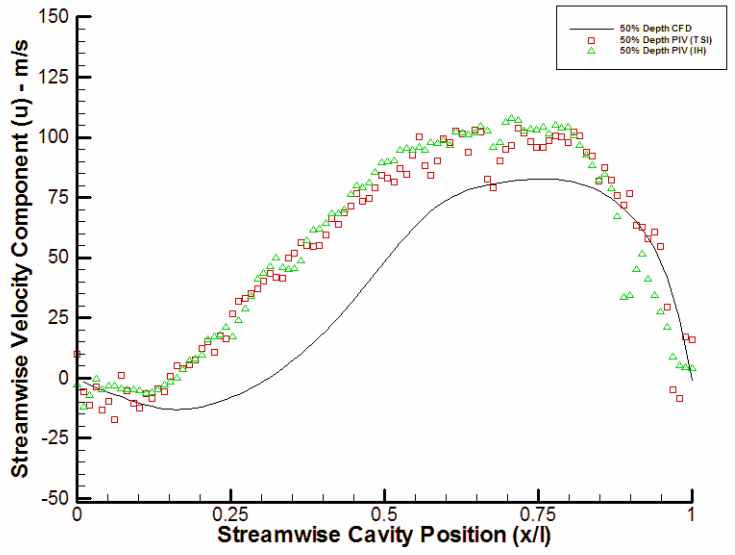

Figure 13 Streamwise Velocity Profile – l/h=14, y/d=0.50